Multiple phases in the e-VPO4O-LiVPO4O-Li2VPO4O system : a combined solid state electrochemistry and diffraction structural study

Mateos Bianchini, Jean-Marcel Ateba Mba, Philippe Dagault, Elena Bogdan, Dany Carlier, Emmanuelle Suard, Christian Masquelier, Laurence Croguennec

Multiple phases in the ε-VPO_4O–$LiVPO_4O$–Li_2VPO_4O system: a combined solid state electrochemistry and diffraction structural study†

M. Bianchini,[abcd] J. M. Ateba-Mba,[abe] P. Dagault,[bd] E. Bogdan,[abd] D. Carlier,[bd] E. Suard,[c] C. Masquelier[ade] and L. Croguennec*[bde]

Polyanionic materials attract great interest in the field of Li-ion battery research thanks to the wide range of possible available compositions, resulting in a great amount of different properties. Tavorite type compositions offer a very rich crystal chemistry, among which $LiVPO_4F$ delivers the highest theoretical energy density. In this work we focus our interest on the homeotypic composition $LiVPO_4O$. This oxyphosphate shows the ability to exploit two redox couples, V^{5+}/V^{4+} at 3.95 V *vs.* Li^+/Li^0 and V^{4+}/V^{3+} at an average potential of 2.3 V *vs.* Li^+/Li^0 upon Li^+ extraction and insertion, respectively. The two domains show marked differences both in the electrochemical signature and in the phase diagram. Here we address for the first time both topics with a combination of electrochemical techniques and *ex situ*/*in situ* X-ray and neutron diffraction and support of density functional theory (DFT) calculations, to get a deep understanding of the behavior of $Li_{1\pm x}VPO_4O$. In the low voltage region, in particular, the formation of intermediate phases and the crystal structure of the end member Li_2VPO_4O are reported for the first time.

DOI: 10.1039/XXXXX

Introduction

Over the past few years, Li-ion batteries have become the leading technology to power portable electronics. The improvement of devices' capabilities has been outstanding and their energy consumption increased accordingly, which implied the necessity to develop batteries with larger capacity and energy density. For this reason many efforts have been devoted to the possible discovery of new materials that could replace commercially available ones. The concern in polyanionic materials,[1] in particular, rose significantly thanks to the success of the triphylite-type $LiFePO_4$, discovered in the mid 90's by Padhi *et al.*, which possesses a capacity of 170 mA h g^{-1} at 3.45 V *versus* Li^+/Li^0, combined with excellent chemical and thermal stability.[2–4] This class of materials is characterized by three-dimensional frameworks built on transition metal cations and polyanions $(XO_4)^{n-}$, resulting in a stable open structure that allows long term reversible lithium extraction and insertion, essential for extensive cycling and safety issues. Other advantages such as the monitoring of a given $M^{n+}/M^{(n+1)+}$ redox couple through the inductive effect[5] and the huge variety of available materials pushed research in the field strongly.[1,6–8]

One of the most interesting developed materials is the vanadium fluorophosphate $LiVPO_4F$, first synthesized by Barker *et al.*,[9,10] that shows one of the highest V^{4+}/V^{3+} redox couples among known polyanionic compositions, reaching 4.2 V *vs.* Li^+/Li^0 (*i.e.* much higher than the well-known anti-Nasicon α-$Li_3V_2(PO_4)_3$ [8,11]). It is based on the Tavorite crystal structure, typical of a wide class of materials[12] and characterized by octahedral chains of transition metal cations, bridged by corner-sharing XO_4 tetrahedra (X = P and S). The high working potential, together with a high capacity of 156 mA h g^{-1} (leading to a theoretical energy density of 655 W h kg^{-1}) and the possibility of exploiting the V^{3+}/V^{2+} redox couple as well (*i.e.* for use in symmetrical cells) made $LiVPO_4F$ a widely studied material and a suitable candidate for commercial exploitation.[13–16] The material most closely related to $LiVPO_4F$ is the vanadium oxyphosphate $LiVPO_4O$[17] which has been shown to possess equally interesting peculiarities.[15] Electrochemically it can also involve two redox couples, which are in this case V^{5+}/V^{4+} at 3.95 V *vs.* Li^+/Li^0 and V^{4+}/V^{3+} around 2.3 V *vs.* Li^+/Li^0. Interestingly, the electrochemical signatures of the two materials show quite different features and their crystal structures as well, although based on the same framework, have marked differences in the lithium ion distribution as well as in the vanadium–oxygen bond lengths.[14–16] In this work, we performed an in-depth study of the electrochemical properties of $LiVPO_4O$, which led to the determination of the phase diagram of VPO_4O–Li_2VPO_4O at 298 K

[a]*Laboratoire de Réactivité et de Chimie des Solides, Université de Picardie Jules Verne, CNRS-UMR#7314, F-80039 Amiens Cedex 1, France*

[b]*CNRS, Univ. Bordeaux, ICMCB, UPR 9048, F-33600 Pessac, France. E-mail: crog@icmcb-bordeaux.cnrs.fr*

[c]*Institut Laue-Langevin, 71 avenue des Martyrs, F-38000 Grenoble, France*

[d]*RS2E, Réseau Français sur le Stockage Electrochimique de l'Energie, FR CNRS#3459, F-80039 Amiens Cedex 1, France*

[e]*ALISTORE-ERI, FR CNRS#3104, F-80039 Amiens Cedex 1, France*

† Electronic supplementary information (ESI) available. See DOI: 10.1039/XXXXX

through electrochemical oxidation (Li^+ extraction) and reduction (Li^+ insertion) reactions.

Experimental

$LiVPO_4O$ was prepared *via* a one-step ceramic route, using V_2O_3 as a vanadium precursor together with $NH_4H_2PO_4$ and Li_3PO_4. All the details about the synthesis and structural determination have already been reported elsewhere.[15] The obtained phase is pure, as can be seen in Fig. 1, and it can be indexed as expected in the triclinic space group $P\bar{1}$. High resolution scanning electron microscopy (SEM) analysis of Pd-metalized samples was performed using a Hitachi S-4500 microscope. The SEM micrographs (the inset of Fig. 1) reveal a primary particle size of about 1 μm with agglomerates of about 5–6 μm.

Electrodes were prepared by ball-milling (SPEX) $LiVPO_4O$ with Carbon Super P (85 : 15 wt% unless specified otherwise). For batteries cycled in coin cells, PVdF was added as a binder (12 wt%) according to the Bellcore protocol,[18] while *in situ* measurements were carried out using directly a mixture of $LiVPO_4O$ and Carbon Super P. As an electrolyte, 1 M $LiPF_6$ in ethylene carbonate (EC)–dimethyl carbonate (DMC) (1 : 1) was used (LP30). *In situ* measurements were performed using a Bruker D8 diffractometer with Cu-K$\alpha_{1,2}$ wavelengths or a PANalytical Empyrean diffractometer with a Cu-Kα_1 setting. In the first case, lithium batteries were prepared in a custom-made *in situ* cell,[19,20] able to perform both in reflection and transmission geometry. Reflection was used in our case. The same geometry but with a custom modified *in situ* cell was used in the second case.

The end members VPO_4O and Li_2VPO_4O were chemically prepared from $LiVPO_4O$. In the first case, it was oxidized with a strong oxidizing agent, nitronium tetrafluoroborate (NO_2BF_4) in acetonitrile media. The resulting yellow powder was then sealed in a 0.2 mm diameter capillary and X-ray diffraction was performed on a PANalytical diffractometer (Empyrean, Cu K$\alpha_{1,2}$) in Debye–Scherrer geometry. In the second case, $LiVPO_4O$ was reduced with $LiAlH_4$ in tetrahydrofuran. The resulting dark gray powder was then sealed in a 0.3 mm diameter capillary and X-ray diffraction was performed on the same diffractometer. Inductively coupled plasma atomic emission spectroscopy (ICP-AES) was used to check the resulting stoichiometry. Neutron diffraction was also carried out on Li_2VPO_4O. The powder was put in a 6.5 mm diameter cylindrical vanadium sample holder and measured at $\lambda = 1.594$ Å on the high-resolution powder diffractometer D2B at Institut Laue-Langevin. Data analysis and structural refinements using the Rietveld method[21] were performed thanks to the FULLPROF suite.[22]

We calculated the total energies using the Generalized Gradient Approximation (GGA) (PBE, the 1996 functional of Perdew, Burke and Ernzerhof)[23] and GGA + U method, using the Projector Augmented Wave (PAW) method[24] as implemented in the Vienna Ab Initio Simulation Package (VASP[25]). The DFT + U method (LDA + U or GGA + U, with LDA, Local-Density Approximations) allows treating more accurately strongly correlated systems, such as transition metals or rare earth-based materials.[26,27] In our study, Dudarev's approach was used to perform GGA + U. The effective on site Coulomb (U) and exchange (J) parameters were not input separately as only the difference $U_{eff} = (U - J)$ is meaningful. Here U_{eff} values of 0, 3, 4 and 4.5 eV were used. A plane wave cutoff energy of 600 meV and a 6 × 6 × 6 k-point grid were used to let the total energies converge by less than 5 meV per unit cell.

Results and discussion

1 High voltage domain

The ability of $LiVPO_4O$ to deintercalate lithium ions from its crystal structure by exploiting the vanadium redox couple V^{4+}/V^{5+} has been addressed in the past focusing mainly on the orthorhombic β-$LiVPO_4O$ phase.[28,29] The triclinic Tavorite-based form of $LiVPO_4O$ has been thought to possess poor electrochemical properties instead,[15,30] the extraction of Li^+ occurring at an average potential of 3.95 V *versus* Li^+/Li^0 at C/50 regime (Fig. 2). Li^+ extraction leads upon first charge to a global composition of "$Li_{0.5}VPO_4O$", raising the question whether (i) such a composition is actually the stable one obtained upon oxidation or (ii) the reaction could not be completed because of the poor electrochemical reactivity of $LiVPO_4O$, which is attributed mainly to its low electrical conductivity.[28,30]

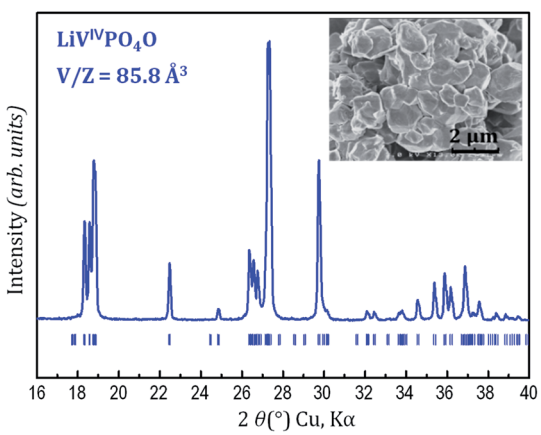

Fig. 1 X-ray diffraction pattern of phase-pure $LiVPO_4O$, indexed in the $P\bar{1}$ space group. The inset is the SEM micrograph.

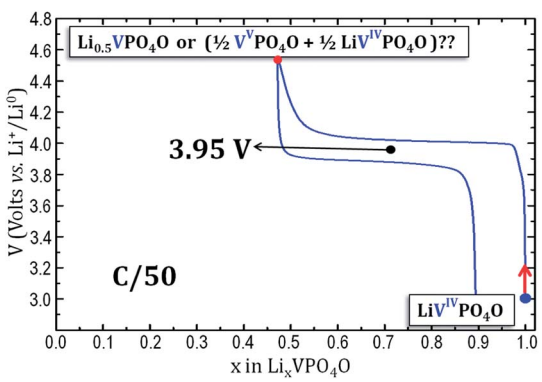

Fig. 2 Galvanostatic cycling of a Li//LP30//$LiVPO_4O$ cell at C/50 from 3 V to 4.6 V *vs.* Li^+/Li^0.

To address this question, *in situ* X-ray diffraction was performed during lithium deintercalation from $LiVPO_4O$ at a C/50 rate. Diffraction patterns were recorded for 70 minutes each in the angular domain [13–44°] during galvanostatic cycling. The result of such a measurement is reported in Fig. 3. The phase diagram clearly shows that when the global composition "$Li_{0.5}VPO_4O$" is reached at 4.5 V *vs.* Li, the initial phase has not completely disappeared. Indeed, the diffraction peak in the 30°–2θ region loses intensity to about half of its original value. Upon discharge, the same battery shows reversible behavior, with the peak intensities of the $LiVPO_4O$ phase returning to values very close to the initial ones.

This first observation was a strong hint suggesting that the intermediate composition $Li_{0.5}VPO_4O$ did not exist as a stable single phase. Besides, DFT calculations (described later in the paper) showed that the $Li_{0.5}VPO_4O$ phase is not stable *versus* $LiVPO_4O$ and VPO_4O, indicating that full extraction of Li^+ from $LiVPO_4O$ is possible (Fig. S1†). A close look at the (200) diffraction peak reveals additional important information. In fact its Full Width at Half Maximum (FWHM) grows continuously during charge and it broadens also during subsequent discharge, reaching a value about 40% larger than the initial one after the first electrochemical cycle. The growth of the peak's FWHM indicates the shrinkage of the crystallite coherent domain size, which can be linked to a decrease of particles' size and therefore to a possible enhancement of the electrochemical reactivity of $LiVPO_4O$. Unfortunately we could not verify the presence of possible anisotropic broadenings because of the limited resolution and angular domain. To get better insight into this behavior, subsequent $LiVPO_4O$ charge/discharge cycles were recorded and the results are shown in Fig. 4. From cycle 1 to cycle 30 a continuous increase of the delivered capacity is observed, from the initial value of 78 mA h g^{-1} to about 135 mA h g^{-1} (in comparison to a theoretical capacity of 159 mA h g^{-1}), corresponding also to a drastic decrease of the battery polarization. This supports the hypothesis that big agglomerated particles of $LiVPO_4O$ do not fully contribute to the electrochemical reaction but show that the kinetics can be significantly improved. Such an improvement in electrochemical properties agrees with previous observations of an increased capacity of orthorhombic β-$LiVPO_4O$ when ball milled.[29]

The study of the end reaction member VPO_4O has also been carried out, since it is a material with a rich crystal chemistry, as witnessed by the existence of many different polymorphs reported in the literature (Table 1) showing interesting properties in the field of batteries but also of catalysis.[31] Among many possibilities, the preparation of VPO_4O from $LiVPO_4O$, both chemically and electrochemically, results in the monoclinic ε-VPO_4O phase. Such a compound has already been reported in the literature with contradictory results since different authors propose different space groups and crystal structures. Indeed, the ε-VPO_4O polymorph had first been indexed in the monoclinic $P2_1/n$ space group and its structure

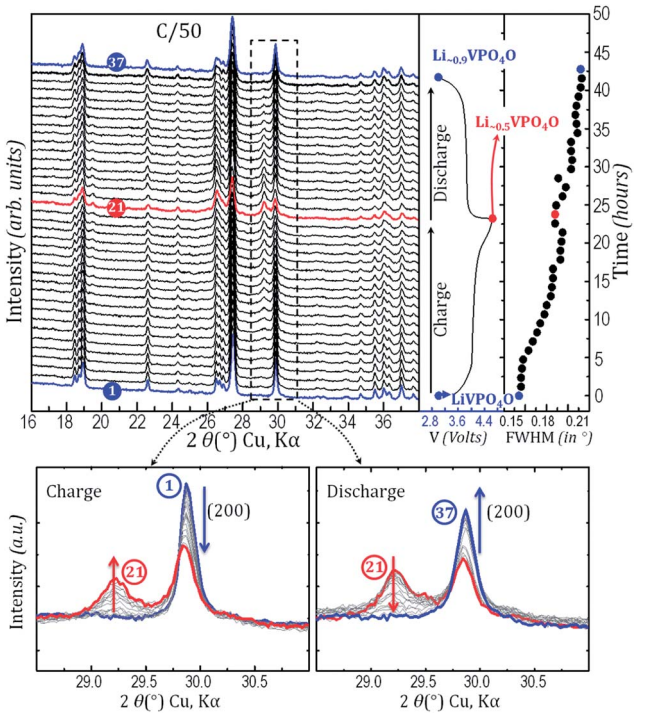

Fig. 3 *In situ* XRD patterns (left) of a Li//LP30//$LiVPO_4O$ cell upon galvanostatic charge and discharge (middle) at C/50 up to 4.5 V. The evolution of the FWHM of the (200) peak (30°) is shown on the top right part of the figure. An enlarged view of the 28.5–31° region is also given at the bottom.

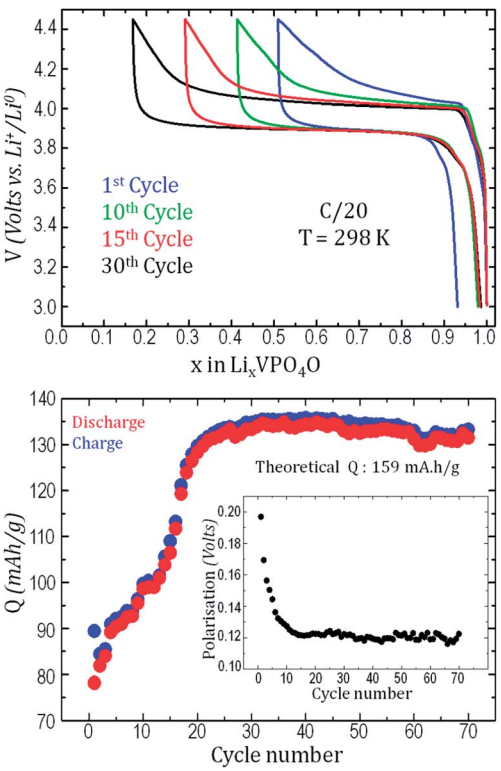

Fig. 4 (Top) Different cycles (rate C/20) for a Li//LP30//$LiVPO_4O$ cell. The electrode active mass is 3.8 mg. (Bottom) Charge and discharge capacities of the cell *versus* number of cycles and respective polarization (inset).

Table 1 Structural data on different polymorphs of VPO_4O. Space groups and vanadium–oxygen bond lengths are reported

	V=O (Å)	V–O (Å)	Symmetry	Space group
ε-VPO_4O (this work)	1.59	2.51	Monoclinic	*Cc*
ε-VPO_4O (this work)	1.59	2.51	Monoclinic	$P2_1/n$
ε-VPO_4O (ICSD no. 415924)	1.57	2.56	Monoclinic	*Cc*
δ-VPO_4O (ICSD no. 420073)	1.62	1.84	Tetragonal	$P4_2/mbc$
γ-VPO_4O (ICSD no. 415213)	1.50 1.62	2.70 1.81	Orthorhombic	*Pbam*
β-VPO_4O (ICSD no. 9413)	1.56	2.59	Orthorhombic	*Pnma*
α_{II}-VPO_4O (ICSD no. 2889)	1.58	2.86	Tetragonal	*P4/n*
α_I-VPO_4O (ICSD no. 108983)	1.63	2.48	Tetragonal	*P4/n*

was determined.[32,33] More recently, a second indexation in the *Cc* space group was found[34] and the two structures were compared, resulting in a less distorted *Cc* structure. For this reason we performed careful X-ray diffraction experiments on VPO_4O powder, chemically obtained from oxidation of $LiVPO_4O$ and sealed in a capillary. The measured XRD pattern is shown in Fig. 5.

The possible space groups found from automatic indexation of XRD data are *Cc*, *C2/c* and $P2_1/n$. In order to investigate theoretically the phase stability of the different structural hypotheses we compared the total energies resulting from DFT calculations using GGA and GGA + *U* methods. For VPO_4O with the $P2_1/n$ and *Cc* space groups, we used as initial structures those previously reported.[33,34] For VPO_4O with the *C2/c* space group, we used as an initial structure the one of VPO_4F [14] replacing F by O. We also considered a cell with a $P\bar{1}$ space group using the cell of $LiVPO_4O$ and removing all Li^+ ions. All structures were fully relaxed and the corresponding structural parameters are given in Table S2 (ESI†). The lower energy was obtained for VPO_4O in *Cc* in both GGA and GGA + *U* calculations. In Table S1† we give the formation energy per formula unit for each case *versus* the most stable phase. It appears that VPO_4O described in $P2_1/n$ is only slightly less stable than the one described in *Cc* by only 7 meV per formula unit. VPO_4O described in $P\bar{1}$ is more clearly less stable by 27 meV per formula unit. The largest energy difference is obtained for VPO_4O described in *C2/c* (343 meV per formula unit) where all V^{5+} ions are located in the center of the VO_6 octahedra with similar V–O distances along the chains as observed in $VPO_4 \cdot H_2O$,[35] where the oxidation state is 3+, or in VPO_4F, where it is 4+.[14] This indicates that the formation of short V–O (vanadyl type) and long V–O bonds along the chains, as it is the case for the three other structural hypotheses, strongly stabilizes the structure.

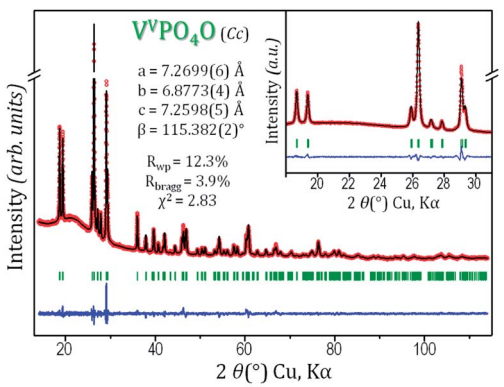

Fig. 5 XRD measurement and Rietveld refinement of a ε-VPO_4O powder sealed in a 0.2 mm capillary.

Based on our theoretical study, the structure was refined (Fig. 5) thanks to the Rietveld method in the space groups *Cc* or $P2_1/n$, leading to better refined parameters for the *Cc* crystal structure (Table S3 in the ESI†), in agreement with the theoretical phase stability. Cell parameters were refined to a = 7.2699(6) Å, b = 6.8773(4) Å, c = 7.2598(5) Å, and β = 115.382(2)° (vol = 327.93(4) Å^3) and the structure showed the expected alternated long and short V–O distances along the octahedral vanadium chains, with bond lengths of 2.51(2) Å and 1.59(2) Å, respectively. Small distortions are observed for both the in-plane V–O distances (between 1.85(2) Å and 1.93(3) Å) and P–O distances (1.55(2) Å, 1.56(4) Å, 1.55(3) Å and a shorter one of 1.48(4) Å, in agreement with the structure reported by Girgsdies *et al.*[34]). More recently, this result was further confirmed,[36] leaving no more doubts about the satisfactory description of ε-VPO_4O in the monoclinic *Cc* space group.

2 Low voltage domain

The open framework structure of $LiVPO_4O$ allows for Li^+ insertion as well until the composition Li_2VPO_4O is reached, exploiting the redox couple V^{4+}/V^{3+}. The corresponding electrochemical galvanostatic intermittent titration technique (GITT) data have been previously published by some of us.[15] As discussed above, the synthesis of $LiVPO_4O$ leads to the formation of 1–2 μm particles, highly agglomerated (5–6 μm, Fig. 1). SPEX ball-milling has been performed so as to decrease the particle size and, as illustrated in Fig. 6 (for similar electrode masses (≈4 mg)), the longer the grinding process is, the higher the electrochemical reactivity will be. This significant improvement is achieved due to the smaller size of the obtained particles, which can be observed as a broadening of the diffraction lines (Fig. 6, insets). Therefore, for a sample milled for a long time (30′ here), a discharge capacity close to the theoretical one can be achieved together with good reversibility, while for shorter milling time the capacity decreases and strong irreversibility is observed, probably due to limited diffusion within the large particles.

The electrochemical data show 3 peculiar features: the first long voltage–composition plateau at 2.45 V *vs.* Li^+/Li^0 between $LiVPO_4O$ and $Li_{1.5}VPO_4O$, the second "pseudo-plateau" at 2.21 V *vs.* Li^+/Li^0, from $Li_{1.5}VPO_4O$ to $Li_{1.75}VPO_4O$ and the final short plateau at 2.04 V *vs.* Li^+/Li^0 to reach the end member Li_2VPO_4O. The reversible reactions involved are:

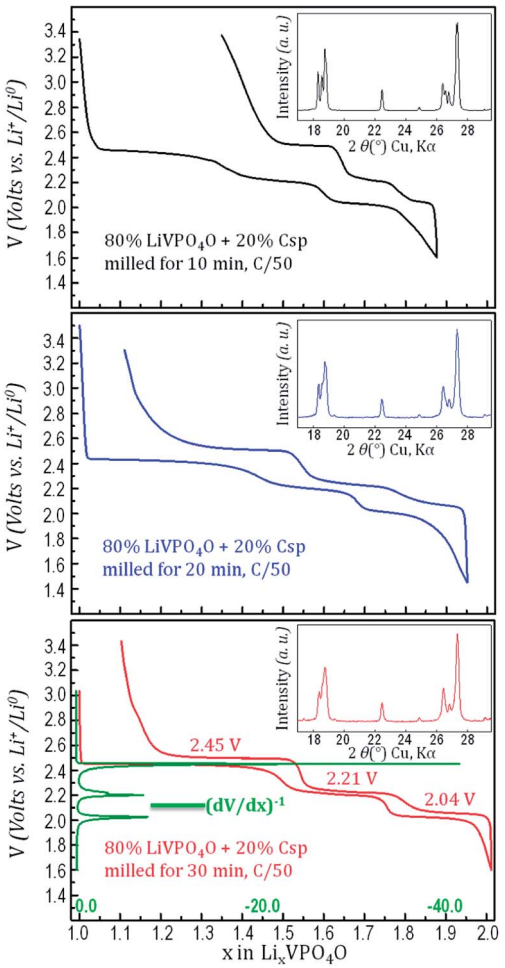

Fig. 6 Galvanostatic cycling for three different SPEX ball-milling durations of a mixture of 80 wt% $LiVPO_4O$ and 20 wt% Csp. The cycle at the bottom is shown with the respective derivative curve (green). Diffractograms (insets) of the respective crystalline powders obtained after milling are reported.

$$LiV^{IV}PO_4O + 0.5Li^+ + 0.5e^- \Leftrightarrow Li_{1.5}V^{3.5+}PO_4O$$

$$Li_{1.5}V^{3.5+}PO_4O + 0.25Li^+ + 0.25e^- \Leftrightarrow Li_{1.75}V^{3.25+}PO_4O$$

$$Li_{1.75}V^{3.25+}PO_4O + 0.25Li^+ + 0.25e^- \Leftrightarrow Li_2V^{III}PO_4O$$

According to the Gibbs phase rule, the first flat voltage–composition plateau suggests a first order reaction, *i.e.* a two-phase reaction between the end members $LiVPO_4O$ and $Li_{1.5}VPO_4O$. This is strongly supported from the derivative curve $(dV/dx)^{-1}$, reported in green at the bottom of Fig. 6 showing an intense narrow peak at 2.45 V. Further Li^+ insertion into $Li_{1.5}VPO_4O$ results in a feature that is not perfectly flat (Fig. S2†), therefore suggesting that a second order mechanism cannot be *a priori* ruled out. The insertion of the last $0.25Li^+$ proceeds again through a similar feature, thus suggesting again a possible solid solution between $Li_{1.75}VPO_4O$ and Li_2VPO_4O.

In situ X-ray diffraction during battery operation was thus chosen to carefully assess the validity of these assumptions. It was performed on a X-ray PANalytical diffractometer equipped with Cu-Kα_1 radiation, allowing high resolution data acquisition which is of key importance given the triclinic symmetry of the structures under investigation. A battery was cycled in a custom-made *in situ* cell with discharge, subsequent charge and a second final discharge of a Li//$LiVPO_4O$ cell at the rate of C/48. Every pattern was recorded in the [17–47°] region for two hours, corresponding to a lithium exchange of 0.04Li each (= 2/48). Fig. 7 shows a contour plot of the whole operando experiment in two selected regions [26–30°] and [40–45°], together with the electrochemical data on the right and an enlarged view of the phase transformations in the [26–30°] region at the bottom. A highly reversible reaction could be achieved, with the full capacity of $LiVPO_4O$ reached during first discharge.

Regarding the phase diagram, the biphasic reaction between $LiVPO_4O$ and $Li_{1.5}VPO_4O$, expected from the derivative curve, could be identified and it can be observed that every pattern is clearly a linear combination of the two end members (patterns #1 and #14, respectively blue and red in Fig. 7).

From a first look at the diffraction patterns the subsequent insertion mechanisms from $Li_{1.5}VPO_4O$ to $Li_{1.75}VPO_4O$ and from $Li_{1.75}VPO_4O$ to $Li_{2.0}VPO_4O$ do not appear straightforward. As previously mentioned, both a solid solution and a series of two 2-phase reactions had to be considered. At first, the single-phase mechanism (solid solution) seems to be the preferred choice since a certain evolution of the cell parameters correlated with a shift of the Bragg positions is clear from the contour plot. Indeed, in the general case, a 2-phase reaction should not allow any important shift of the cell parameters. We therefore simulated the intermediate patterns as a linear combination of the end members (*e.g.* pattern #17 simulated as $x \times$ pattern #14 $+ (1 - x) \times$ pattern #21 and pattern #24 simulated as $x \times$ pattern #21 + $(1 - x) \times$ pattern #27). As shown in Fig. 8, the experimental patterns (#17 and #24) recorded at the middle of each "pseudo-plateau" cannot be fitted considering these linear combinations, which seems thus to exclude the straightforward two-phase reactions $Li_{1.5}VPO_4O \Leftrightarrow Li_{1.75}VPO_4O$ and $Li_{1.75}VPO_4O \Leftrightarrow Li_2VPO_4O$. Subsequently, we thus tried to refine all the patterns from #14 to #27 as single phases with variable cell parameters, using a Le Bail fit since the exact crystal structures are not known (many attempts have been done to isolate the intermediate phases $Li_{1.5}VPO_4O$ and $Li_{1.75}VPO_4O$ to determine their crystal structure, but without success). The cell parameters obtained are plotted in Fig. 9 and those determined for patterns #1, #14, #21, and #27 are reported in Table 2. The lattice parameter variation obtained considering the single-phase model is not fully convincing, since it is not smooth but rather step-like. This suggests the presence of a major phase that dominates the behavior and of a minor one that is almost unseen. Also, the evolution of χ^2 factors (bottom part of Fig. 9) gives a useful indication since the "important" single-phase compositions (patterns #14, #21 and #27) show good fits while those intermediates between them correspond to χ^2 values significantly increased.

We therefore decided to carry on the investigation and to refine the patterns #14, #21 and #27 as single phases, while all intermediate compositions were refined with two phases for

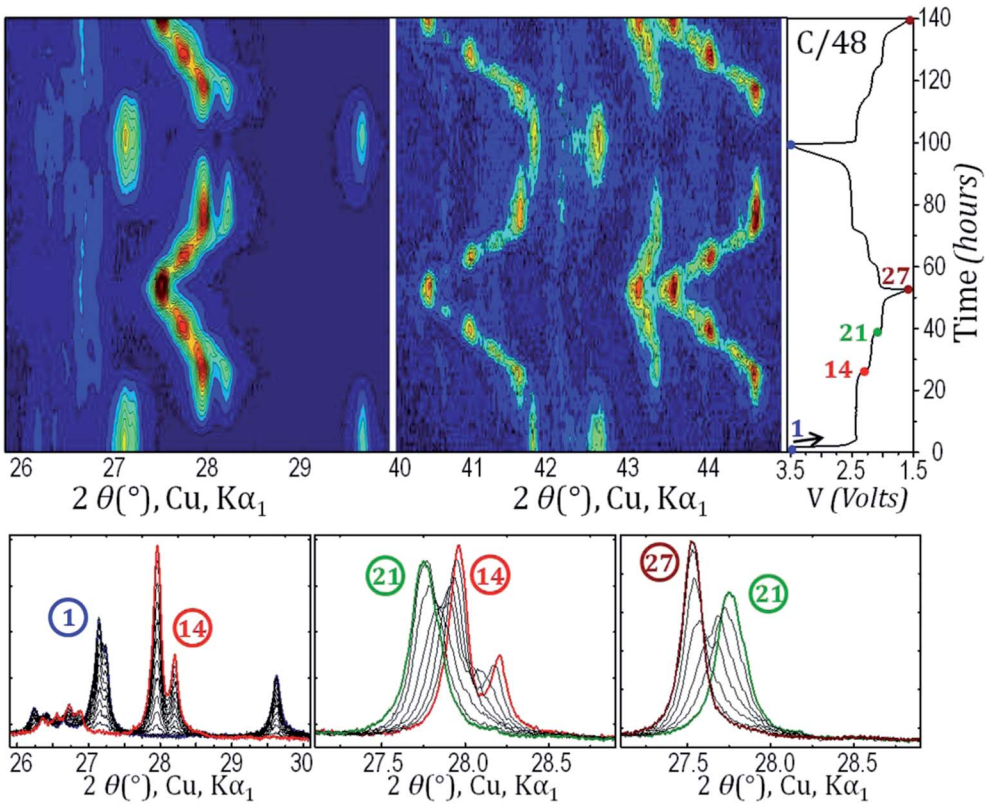

Fig. 7 Operando X-ray diffraction measurement of $LiVPO_4O$ cycled at C/48 rate. The first cycle and a second discharge were recorded. (Top) Contour plot and electrochemical curve. (Bottom) An enlarged view of the [26–30°] or [27–29°] region of the first discharge where important compositions are highlighted (pristine $LiVPO_4O$ (pattern #1, blue), $Li_{1.5}VPO_4O$ (pattern #14, red), $Li_{1.75}VPO_4O$ (pattern #21, green) and Li_2VPO_4O (pattern #27, brown)).

which the cell parameters were allowed to vary (the zero shift was always fixed thanks to a Beryllium diffraction peak used as reference). The result is shown in Fig. 10. Despite the presence of two triclinic phases, it is remarkable that the cell parameters do not vary significantly. This is particularly true for a, b and c, while a certain variation of the angles is observed. Two main reasons can be adduced to justify this behavior. The first one is of experimental nature. Indeed, we cannot expect a perfect accuracy from the proposed Le Bail fit, since there are many Bragg positions composing every apparent peak. As an example, the doublet in the [27.5–28.5°] region (pattern #14, red in Fig. 7) is actually composed of 6 different Bragg positions. When the subsequent patterns are considered and two phases are present, the number of Bragg positions in the same peak becomes 12. The second reason is physical and it deals with the fact that the experimental observation of an evolution of the cell parameters in a two phase reaction is not impossible, and has been recently reported for the $NaFePO_4$–$FePO_4$ system[37] and for the FeOF system.[38] This can have different causes, like important strains at the interface between the transforming phases. Once again, a look at the evolution of the χ^2 factor is relevant, not because of the lower obtained values which are somehow expected having doubled the amount of free parameters, but for the lack of a structure in the χ^2 distribution for the different patterns, which is approximately flat and satisfactory for all of them. Besides, Table 2 reveals another interesting fact. The unit cell volume changes poorly between $LiVPO_4O$ and $Li_{1.5}VPO_4O$ ($\Delta V/V$ = 0.14%), while it changes significantly from $Li_{1.5}VPO_4O$ to Li_2VPO_4O (3.92%). This strong difference may be the explanation for such dissimilar phase behavior between these composition ranges. The transition from $LiVPO_4O$ to $Li_{1.5}VPO_4O$ involves a very small volume change and it can therefore happen *via* a perfect first order reaction. In contrast, the transitions from $Li_{1.5}VPO_4O$ to $Li_{1.75}VPO_4O$ and from $Li_{1.75}VPO_4O$ to Li_2VPO_4O involve a significant volume change (almost 2% for 0.25 lithium atoms) and they thus take place with significant strain in the material, determining a small but observable variation in the cell parameters.

3 Crystal structure of Li_2VPO_4O

To the best of our knowledge, no detailed description of the crystal structure of Li_2VPO_4O has been reported in the literature so far, besides the values of the cell parameters[39] and the study of lithium ion dynamics using ^6Li 1D selective inversion solid-state nuclear magnetic resonance methods.[40] We prepared Li_2VPO_4O through chemical reduction of $LiVPO_4O$ and measured the resulting powder on a PANalytical Empyrean X-ray diffractometer and subsequently on the high resolution powder neutron diffractometer D2B at ILL. No enrichment of

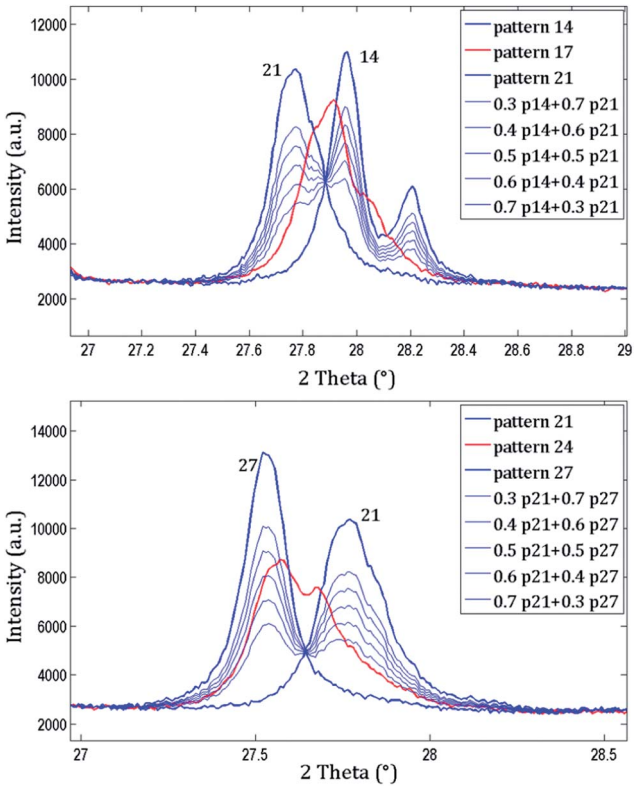

Fig. 8 (Top) Patterns #14 and #21 are considered as extreme members of the biphasic reaction between $Li_{1.5}VPO_4O$ and $Li_{1.75}VPO_4O$. A perfect biphasic reaction is simulated as $x \times$ pattern #14 + $(1 - x) \times$ pattern #21 (x = 0.3, 0.4, 0.5, 0.6, and 0.7). The simulations can be compared with the experimental pattern #17 (red), corresponding to a composition close to $Li_{1.6}VPO_4O$. (Bottom) Patterns #21 and #27 are considered as extreme members of the biphasic reaction between $Li_{1.75}VPO_4O$ and Li_2VPO_4O. A perfect biphasic reaction is simulated as $x \times$ pattern #21 + $(1 - x) \times$ pattern #27 (x = 0.3, 0.4, 0.5, 0.6, and 0.7). The simulations can be compared with the experimental pattern #24 (red), corresponding to a composition close to $Li_{1.87}VPO_4O$.

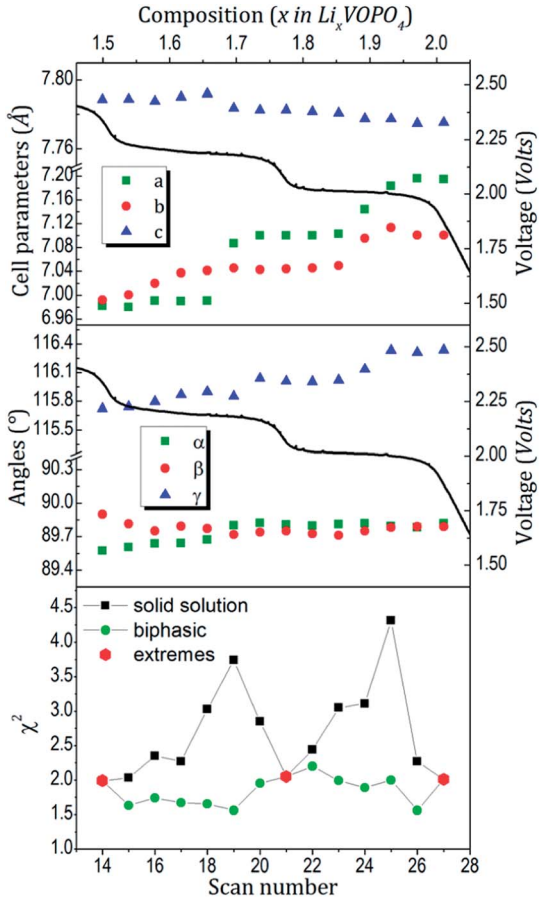

Fig. 9 (Top and middle) Refined cell parameters (Le Bail fit) for a single phase solid solution between the compositions $Li_{1.5}VPO_4O$ and Li_2VPO_4O. (Bottom) χ^2 parameters from the Le Bail fit of the XRD scans from #14 to #27. χ^2 for a single phase solid solution is compared to χ^2 for a sequence of two biphasic reactions. End members (in red) are $Li_{1.5}VPO_4O$, $Li_{1.75}VPO_4O$ and Li_2VPO_4O.

the sample was performed; Li with natural abundance was used for neutron diffraction. The patterns were indexed in the triclinic $P\bar{1}$ space group and the cell parameters retrieved are: a = 7.1989(4) Å, b = 7.1012(3) Å, c = 7.7771(3) Å, α = 89.824(3)°, β = 89.812(3)°, and γ = 116.319(3)°. The resulting volume of the unit cell is 356.36(3) Å^3. A transformation $a' = b$, $b' = a$, $c' = -c$, $\alpha' = 180 - \alpha$, $\beta' = 180 - \beta$ and $\gamma' = \gamma$ can be used to find a more standard triclinic setting, where the cell parameters are a' = 7.1012(3) Å, b' = 7.1989(4), c' = 7.7771(3) Å, α' = 90.176(3)°, β' = 90.188(3)°, and γ' = 116.319(4)°. In this paper, the first setting will be used to allow a better comparison with the structure of $LiVPO_4O$.[15] The obtained parameters are not in good agreement with a previous report[39] but are remarkably similar to those obtained from the end member of the *in situ* XRD experiment described in the previous section (Table 2). As generally expected for lithium intercalation and vanadium reduction, the unit cell volume of Li_2VPO_4O (352.36(2) Å^3) is larger than the value obtained for $LiVPO_4O$ (342.03(1) Å^3) and for VPO_4O (327.93(4) Å^3). In both cases the insertion of one lithium ion expands the unit cell by about 4% of its initial volume. Atomic coordinates of Li_2VPO_4O were subsequently located thanks to the FOX software[41] and the X-ray and neutron patterns refined with the Rietveld method. Li_2VPO_4O shows a double cell analogous to that of $LiVPO_4O$ and this doubles the number of free parameters to be refined. Because of this and since the two different probes are sensitive to different structural parameters, both patterns were exploited to obtain the final crystal structure, *via* step by step refinements between the X-ray and neutron patterns. For instance, oxygen positions obtained from the X-ray pattern are not accurate because of the high number of oxygen coordinates (30 independent parameters) and the limited sensitivity of X-rays to light elements, whereas vanadium is transparent to neutrons.

The results obtained from the dual refinement of X-ray and neutron diffraction data are shown in Fig. 11 and the resulting representation of the crystal structure in Fig. 12. The refined parameters are reported in Table 3. Bond length distances and polyhedra coordination are reported in Table 4.

Lithium's fractional atomic coordinates were determined thanks to Fourier difference maps, their location being not straightforward. Indeed, the first 4 lithium positions (Li1 and

Table 2 Cell parameters of selected Li_xVPO_4O compositions, refined in the space group $P\bar{1}$

	a (Å)	b (Å)	c (Å)	α (°)	β (°)	γ (°)	V (Å^3)
$LiVPO_4O$ (ref. 15)	6.7320(1)	7.1942(1)	7.9204(1)	89.843(1)	91.272(1)	116.886(4)	342.03(1)
$LiVPO_4O$ (*in situ*)	6.7341(4)	7.1959(5)	7.9177(4)	89.812(5)	91.277(5)	116.910(5)	342.04(3)
$Li_{1.5}VPO_4O$ (*in situ*)	6.9820(3)	6.9922(3)	7.7886(3)	89.573(5)	89.901(6)	115.722(4)	342.54(2)
$Li_{1.75}VPO_4O$ (*in situ*)	7.1002(4)	7.0443(3)	7.7826(4)	89.809(4)	89.753(5)	116.010(6)	349.82(3)
Li_2VPO_4O (*in situ*)	7.1948(6)	7.1009(7)	7.7753(7)	89.820(3)	89.791(4)	116.337(5)	356.00(6)
Li_2VPO_4O (chem.)	7.1989(4)	7.1012(3)	7.7771(3)	89.824(3)	89.812(3)	116.319(3)	356.36(2)

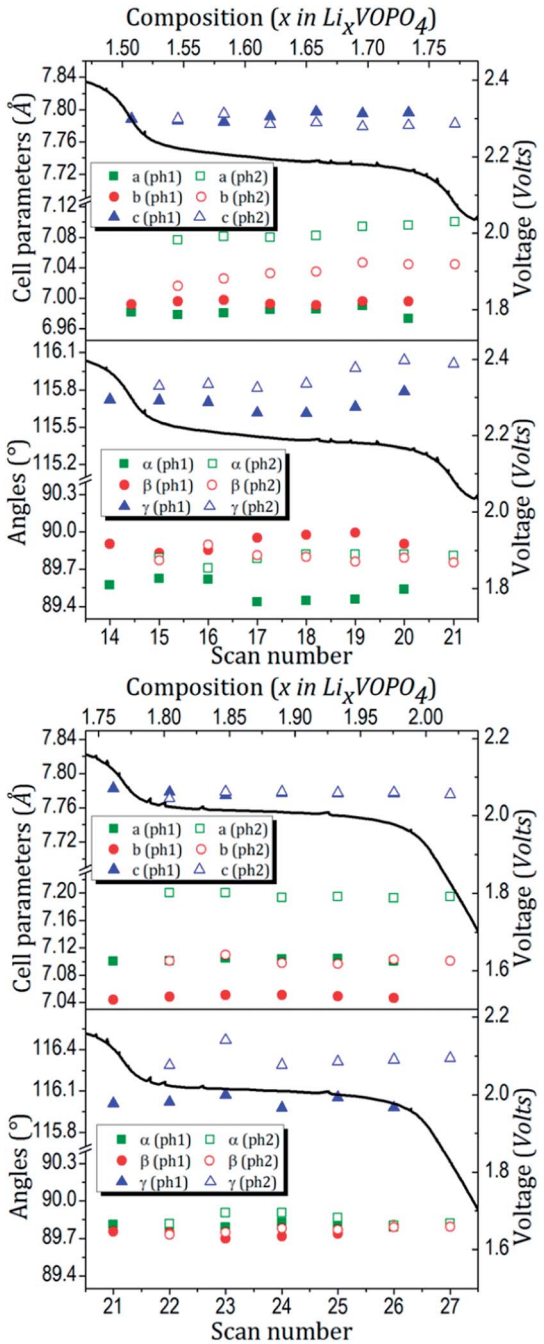

Fig. 10 Refined cell parameters (Le Bail fit) for a sequence of two biphasic reactions between the compositions $Li_{1.5}VPO_4O$ and $Li_{1.75}VPO_4O$ (top) and between $Li_{1.75}VPO_4O$ and Li_2VPO_4O (bottom).

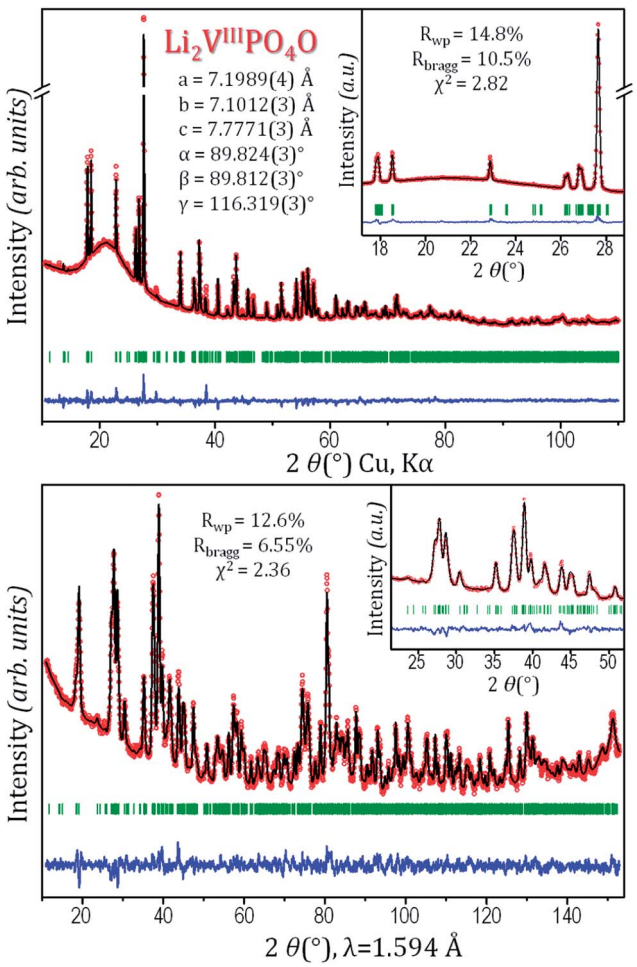

Fig. 11 (Top) XRD measurement and Rietveld refinement of Li_2VPO_4O powder in a 0.3 mm diameter capillary. (Bottom) Neutron diffraction measurement and Rietveld refinement of Li_2VPO_4O placed in a 6.5 mm diameter vanadium container.

Li2, Wyckoff positions 1c and 1h, and Li3 and Li4, positions 2i) emerged quite clearly from the maps. The last site(s), required to give the correct stoichiometry, was less easily detectable. Finally, the best solution was found from the map with the Li5 atom placed in a 2i site. As can be observed in Table 4, V and P environments are in line with those expected, although with significant error bars due to the large number of refined parameters; lithium local environments are also equally plausible, despite two short Li–O distances. No Li–Li distance

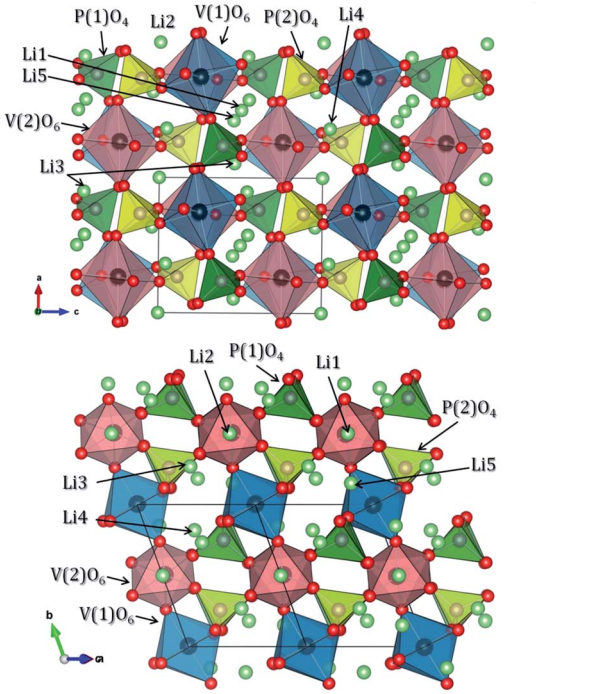

Fig. 12 Crystal structure of Li_2VPO_4O. Lithium positions are indicated.

shorter than 2.3 Å is observed. For all the cations (P^{5+}, V^{3+} and Li^{+}) the bond valences calculated are in very good agreement with those expected from the chemical formula Li_2VPO_4O. Regarding the vanadium environment, the $V(1)O_6$ and $V(2)O_6$ octahedra in Li_2VPO_4O can be compared to what is expected for $V^{3+}O_6$ polyhedra from the survey of Schindler *et al.*[42] Indeed, the 3+ oxidation state in vanadium-centered octahedra is reported to result in an average bond length of 2.01 Å, with a maximum occurrence between 1.98 Å and 2.04 Å and extreme values of 1.88 Å and 2.16 Å. In our structure, the refined values for Li_2VPO_4O give an average value of 2.03 Å for $V(1)O_6$ and of 2.02 Å

Table 3 Structural parameters obtained from Rietveld refinement of XRD and neutron diffraction data of Li_2VPO_4O. Isotropic thermal displacement parameters were constrained to be equal for the same type of atom

Li_2VPO_4O

S.G.: $P\bar{1}$; $Z = 4$
$a = 7.1989(4)$ Å; $b = 7.1012(3)$ Å; $c = 7.7771(3)$ Å
$\alpha = 89.824(3)^\circ$; $\beta = 89.812\ (3)^\circ$; $\gamma = 116.319(3)^\circ$
$V = 356.36\ (3)$ Å^3; $V/Z = 89.09$ Å^3
XRD: $R_{wp} = 14.8\%$; $R_{Bragg} = 10.5\%$; $\chi^2 = 2.82$
Neutrons: $R_{wp} = 12.6\%$; $R_{Bragg} = 6.55\%$; $\chi^2 = 2.36$

Atomic parameters

Atoms	Wyckoff position	Atomic position			Occ	B_{iso}
		x/*a*	*y*/*b*	*z*/*c*		
V(1)	2i	0.748(3)	−0.004(3)	−0.752(3)	1	1.5(2)
V(2)	2i	0.734(3)	−0.505(3)	−0.755(3)	1	2.5(2)
P(1)	2i	0.24(1)	−0.248(9)	−0.612(8)	1	0.8(2)
P(2)	2i	0.27(1)	−0.743(9)	−0.885(8)	1	0.8(2)
O(1)	2i	0.563(5)	−0.910(5)	−0.310(4)	1	0.98(5)
O(2)	2i	0.07(1)	−0.359(9)	−0.755(6)	1	0.98(5)
O(3)	2i	0.721(7)	−0.591(8)	−0.499(6)	1	0.98(5)
O(4)	2i	0.161(8)	−0.117(7)	−0.496(7)	1	0.98(5)
O(5)	2i	0.232(9)	−0.259(8)	−0.152(7)	1	0.98(5)
O(6)	2i	0.064(5)	−0.883(5)	−0.784(4)	1	0.98(5)
O(7)	2i	0.230(7)	−0.588(8)	−0.993(6)	1	0.98(5)
O(8)	2i	0.728(8)	−0.260(8)	−0.652(7)	1	0.98(5)
O(9)	2i	0.57(1)	−0.354(9)	−0.259(6)	1	0.98(5)
O(10)	2i	0.337(8)	−0.877(7)	−0.008(7)	1	0.98(5)
Li(1)	1d	1/2	1/2	1/2	1	2.2(7)
Li(2)	1h	0	1/2	0	1	2.2(7)
Li(3)	2i	0.10(1)	0.27(1)	0.46(1)	1	2.2(7)
Li(4)	2i	0.36(1)	0.82(1)	0.04(1)	1	2.2(7)
Li(5)	2i	0.42(1)	0.15(1)	0.45(1)	1	2.2(7)

Table 4 Significant bond length distances of Li_2VPO_4O obtained from Rietveld refinement of XRD and neutron diffraction data. Only distances shorter than 2.5 Å are considered. V–O distances along the chains are highlighted in **bold**. Polyhedral distortion is calculated as $\Delta = \frac{1}{N}\sum_{i=1}^{N}\left(\frac{d_i - \langle d\rangle}{\langle d\rangle}\right)^2$, bond valences as previously reported[40]

Li_2VPO_4O

	V(1)	V(2)	P(1)	P(2)	Li(1)	Li(2)	Li(3)	Li(4)	Li(5)
Coord.	6	6	4	4	6	6	4	5	6
O(1)	2.09(4)	—	1.51(7)	—	—	—	—	2.17(7)	2.23(9), 2.09(9)
O(2)	—	2.17(6)	1.57(8)	—	—	2.11(5) × 2	—	2.48(8)	—
O(3)	—	2.07(5)	1.57(9)	—	1.96(6) × 2	—	2.10(9)	—	2.15(9)
O(4)	2.10(5)	—	1.55(9)	—	—	—	1.75(9)	—	2.03(9)
O(5)	**1.96(7)**	**1.94(7)**	—	—	—	2.13(5) × 2	—	1.75(8)	—
O(6)	2.06(4)	—	—	1.56(6)	—	—	2.15(8)	—	—
O(7)	—	2.04(5)	—	1.50(9)	—	2.01(6) × 2	—	—	—
O(8)	**1.92(7)**	**1.93(7)**	—	—	2.12(5) × 2	—	1.93(9)	—	2.21(13)
O(9)	—	1.95(6)	—	1.56(8)	2.10(5) × 2	—	—	—	2.07(10)
O(10)	2.03(5)	—	—	1.58(9)	—	—	—	2.29(9), 2.01(9)	—
Distortion	11.1×10^{-4}	18.4×10^{-4}	2.6×10^{-4}	4.1×10^{-4}	10.9×10^{-4}	2.6×10^{-4}	62.0×10^{-4}	135×10^{-4}	11.9×10^{-4}
Bond-valence	2.8(2)	2.9(2)	4.8(6)	4.8(5)	1.22(8)	1.13(7)	1.1(2)	1.0(1)	1.0(1)

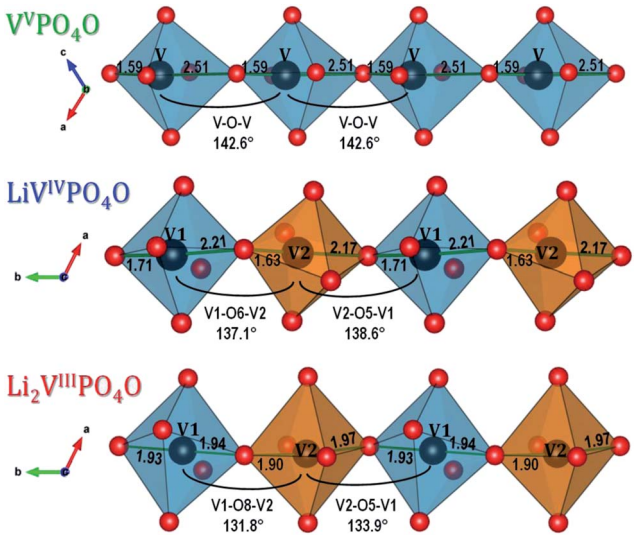

Fig. 13 Octahedral chains of VPO_4O (top), $LiVPO_4O$ (middle) and Li_2VPO_4O (bottom), with V–O distances and V–O–V angles along the chains.

for $V(2)O_6$, with all the V–O bond lengths in good agreement with the expected values. It is also interesting to note how the bonds along the chains are significantly shorter than the in-plane bonds in the octahedra.

The V–O octahedral chains of the 3 end-members VPO_4O, $LiVPO_4O$ and Li_2VPO_4O are displayed in Fig. 13. The general trend is a transition from long and short alternated V–O distances along the chains for V in the 5+ oxidation state (ionic radius 0.54 Å) to progressively more homogeneous ones while the oxidation state decreases to 4+ and then 3+ (ionic radii 0.58 Å and 0.64 Å respectively). The presence of long and short alternated V–O distances observed for the V^{4+} and V^{5+} phases is due to the formation of the vanadyl-type bond within the VO_6 octahedra, that is not observed for the V^{3+}-rich phase.[42] The V–O–V angles, as well, diminish from high values (142.6°) to smaller ones (131–134°), while the octahedra show less and less distortions. Consequently and interestingly, the length of the chain diminishes on going from VPO_4O to $LiVPO_4O$ and to Li_2VPO_4O as witnessed by the strong contraction of the *b* lattice parameter from $LiVPO_4O$ (7.196 Å) to Li_2VPO_4O (7.101 Å) while the unit-cell volume increases (from 342.03 $Å^3$ for $LiVPO_4O$ to 356.44 $Å^3$ for Li_2VPO_4O).

Conclusion

In this work we have detailed for the first time how the Tavorite oxy-phosphate $LiVPO_4O$ transforms after both lithium extraction and insertion. From the electrochemical point of view, we showed how the particles' size is the crucial property to achieve full capacity from such a material and how this capacity can be improved. In particular, this can happen either spontaneously during battery operation (electrochemical grinding observed here at high voltage), or through ball-milling (here carried out to improve the low voltage reactivity). From the structural point of view, we have used X-ray and neutron diffraction, *in situ* and *ex situ*, to follow carefully the structural changes of Li_xVPO_4O ($0 < x < 2$). In the high voltage domain, we observed a two-phase reaction involving the redox couple V^{5+}/V^{4+} between pristine $LiVPO_4O$ and the end member ε-VPO_4O, which has been confirmed to belong to the *Cc* space group. Furthermore, in the low potential domain the V^{4+}/V^{3+} redox couple is confirmed to be active and it is shown to possess a very rich series of phase transformations upon lithium intercalation. The occurrence of a solid solution or a biphasic reaction mechanism is discussed. Finally, the end member of this reaction, Li_2VPO_4O, has been isolated and its triclinic crystal structure is determined in detail.

Acknowledgements

The authors thank Benoit Mortemard de Boisse, Cathy Denage and Eric Lebraud (ICMCB) for fruitful discussions and technical support, Marie Liesse Doublet (ICG Montpellier) for fruitful discussions, as well as the ILL (Grenoble, France) for the beam time granted on the D2B high resolution neutron diffractometer and for the PhD grant of M.B. The authors also acknowledge the financial support of the ANR program PROGELEC (HIPOLITE no. ANR-12-PRGE-0005-02), Région Aquitaine, Région Picardie and ILL.

References

1 C. Masquelier and L. Croguennec, *Chem. Rev.*, 2013, **113**, 6552–6591.
2 A. K. Padhi, K. S. Nanjundaswamy and J. B. Goodenough, *J. Electrochem. Soc.*, 1997, **144**, 1188–1194.
3 A. K. Padhi, K. S. Nanjundaswamy, C. Masquelier, S. Okada and J. B. Goodenough, *J. Electrochem. Soc.*, 1997, **144**, 1609–1613.
4 A. Yamada, H. Koizumi, S. I. Nishimura, N. Sonoyama, R. Kanno, M. Yonemura, T. Nakamura and Y. Kobayashi, *Nat. Mater.*, 2006, **5**, 357–360.
5 A. Manthiram and J. B. Goodenough, *J. Power Sources*, 1989, **26**, 403–408.
6 N. Recham, J.-N. Chotard, L. Dupont, C. Delacourt, W. Walker, M. Armand and J.-M. Tarascon, *Nat. Mater.*, 2009, **9**, 68–74.
7 Z. Gong and Y. Yang, *Energy Environ. Sci.*, 2011, **4**, 3223–3242.
8 S. Patoux, C. Wurm, M. Morcrette, G. Rousse and C. Masquelier, *J. Power Sources*, 2003, **119**, 278–284.
9 J. Barker, M. Y. Saidi and J. L. Swoyer, *J. Electrochem. Soc.*, 2003, **150**, A1394–A1398.
10 J. Barker, R. K. B. Gover, P. Burns, A. Bryan, M. Y. Saidi and J. L. Swoyer, *J. Power Sources*, 2005, **146**, 516–520.
11 J. Gaubicher, C. Wurm, G. Goward, C. Masquelier and L. Nazar, *Chem. Mater.*, 2000, **12**, 3240–3242.
12 B. L. Ellis, W. M. Makahnouk, W. Rowan-Weetaluktuk, D. Ryan and L. F. Nazar, *Chem. Mater.*, 2009, **22**, 1059–1070.
13 H. Huang, T. Faulkner, J. Barker and M. Saidi, *J. Power Sources*, 2009, **189**, 748–751.
14 B. L. Ellis, T. Ramesh, L. J. Davis, G. R. Goward and L. F. Nazar, *Chem. Mater.*, 2011, **23**, 5138–5148.

15 J.-M. Ateba Mba, C. Masquelier, E. Suard and L. Croguennec, *Chem. Mater.*, 2012, **24**, 1223–1234.
16 J.-M. Ateba Mba, L. Croguennec, N. I. Basir, J. Barker and C. Masquelier, *J. Electrochem. Soc.*, 2012, **159**, A1171–A1175.
17 A. V. Lavrov, V. P. Nikolaev, G. G. Sadikov and M. A. Poraikoshits, *Dokl. Akad. Nauk SSSR*, 1982, **266**, 343–346.
18 D. Larcher, C. Masquelier, D. Bonnin, Y. Chabre, V. Masson, J.-B. Leriche and J.-M. Tarascon, *J. Electrochem. Soc.*, 2003, **150**, A133–A139.
19 J. B. Leriche, S. Hamelet, J. Shu, M. Morcrette, C. Masquelier, G. Ouvrard, M. Zerrouki, P. Soudan, S. Belin, E. Elkaim and F. Baudelet, *J. Electrochem. Soc.*, 2010, **157**, A606–A610.
20 G. Ouvrard, M. Zerrouki, P. Soudan, B. Lestriez, C. Masquelier, M. Morcrette, S. Hamelet, S. Belin, A. M. Flank and F. Baudelet, *J. Power Sources*, 2013, **229**, 16–21.
21 H. M. Rietveld, *J. Appl. Crystallogr.*, 1969, **2**, 65–71.
22 J. Rodriguezcarvajal, *Physica B*, 1993, **192**, 55–69.
23 J. P. Perdew, K. Burke and M. Ernzerhof, *Phys. Rev. Lett.*, 1996, **77**, 3865–3868.
24 G. Kresse and D. Joubert, *Phys. Rev. B: Condens. Matter Mater. Phys.*, 1999, **59**, 1758–1775.
25 G. Kresse and J. Furthmüller, *Phys. Rev. B: Condens. Matter Mater. Phys.*, 1996, **54**, 11169–11186.
26 V. I. Anisimov, J. Zaanen and O. K. Andersen, *Phys. Rev. B: Condens. Matter Mater. Phys.*, 1991, **44**, 943–954.
27 A. Liechtenstein, V. Anisimov and J. Zaanen, *Phys. Rev. B: Condens. Matter Mater. Phys.*, 1995, **52**, R5467–R5470.
28 B. M. Azmi, T. Ishihara, H. Nishiguchi and Y. Takita, *Electrochemistry*, 2003, **71**, 1108–1110.
29 B. M. Azmi, T. Ishihara, H. Nishiguchi and Y. Takita, *J. Power Sources*, 2005, **146**, 525–528.
30 Y. Yang, H. Fang, J. Zheng, L. Li, G. Li and G. Yan, *Solid State Sci.*, 2008, **10**, 1292–1298.
31 R. Gautier, R. Gautier, O. Hernandez, N. Audebrand, T. Bataille, C. Roiland, E. Elkaim, L. Le Polles, E. Furet and E. Le Fur, *Dalton Trans.*, 2013, **42**, 8124–8131.
32 Y. Song, P. Y. Zavalij and M. S. Whittingham, *J. Electrochem. Soc.*, 2005, **152**, A721–A728.
33 T. A. Kerr, J. Gaubicher and L. F. Nazar, *Electrochem. Solid-State Lett.*, 2000, **3**, 460–462.
34 F. Girgsdies, W. S. Dong, J. K. Bartley, G. J. Hutchings, R. Schlögl and T. Ressler, *Solid State Sci.*, 2006, **8**, 807–812.
35 J. Vaughey, W. T. Harrison, A. J. Jacobson, D. P. Goshorn and J. W. Johnson, *Inorg. Chem.*, 1994, **33**, 2481–2487.
36 Z. Chen, Q. Chen, L. Chen, R. Zhang, H. Zhou, N. A. Chernova and M. S. Whittingham, *J. Electrochem. Soc.*, 2013, **160**, A1777–A1780.
37 J. Gaubicher, F. Boucher, P. Moreau, M. Cuisinier, P. Soudan, E. Elkaim and D. Guyomard, *Electrochem. Commun.*, 2014, **38**, 104–106.
38 K. M. Wiaderek, O. J. Borkiewicz, E. Castillo-Martínez, R. Robert, N. Pereira, G. G. Amatucci, C. P. Grey, P. J. Chupas and K. W. Chapman, *J. Am. Chem. Soc.*, 2013, **135**(10), 4070–4078.
39 M. S. Whittingham, Y. Song, S. Lutta, P. Y. Zavalij and N. A. Chernova, *J. Mater. Chem.*, 2005, **15**, 3362–3379.
40 L. J. M. Davis, X. J. He, A. D. Bain and G. R. Goward, *Solid State Nucl. Magn. Reson.*, 2012, **42**, 26–32.
41 R. Cerny and V. Favre-Nicolin, *Powder Diffraction*, 2005, **20**, 359–365.
42 M. Schindler, F. C. Hawthorne and W. H. Baur, *Chem. Mater.*, 2000, **12**, 1248–1259.